ISBN: 978-3-95450-214-1 ISSN: 2673-5490 doi:10.18429/JACoW-IPAC2021-WEPAB289

MACHINE LEARNING BASED SPATIAL LIGHT MODULATOR CONTROL FOR THE PHOTOINJECTOR LASER AT FLUTE

C. Xu*, E. Bründermann, M. J. Nasse, A. Santamaria Garcia, C. Sax, C. Widmann, A.-S. Müller
Karlsruhe Institute of Technology (KIT), Karlsruhe, Germany
A. Eichler, Deutsches Elektronen-Synchrotron DESY, Hamburg, Germany

Abstract

FLUTE (Ferninfrarot Linac- und Test-Experiment) at KIT is a compact linac-based test facility for novel accelerator technology and a source of intense THz radiation. FLUTE is designed to provide a wide range of electron bunch charges from the pC- to nC-range, high electric fields up to 1.2 GV/m, and ultra-short THz pulses down to the fs-timescale. The electrons are generated at the RF photoinjector, where the electron gun is driven by a commercial titanium sapphire laser. In this kind of setup the electron beam properties are determined by the photoinjector, but more importantly by the characteristics of the laser pulses. Spatial light modulators can be used to transversely and longitudinally shape the laser pulse, offering a flexible way to shape the laser beam and subsequently the electron beam, influencing the produced THz pulses. However, nonlinear effects inherent to the laser manipulation (transportation, compression, third harmonic generation) can distort the original pulse. In this paper we propose to use machine learning methods to manipulate the laser and electron bunch, aiming to generate tailor-made THz pulses. The method is demonstrated experimentally in a test setup.

INTRODUCTION

As a versatile test facility, the accelerator FLUTE at KIT is designed to operate with different electron beam types [1]. FLUTE will also be used as a source of broadband terahertz (THz) pulses for proof-of-principle photon science experiments. An appropriate control of the electron bunch could facilitate THz pulses tailored to a specific user requirement. Space charge effects are strong at low energies and dependent on the phase space distribution of the electron bunch, which is determined during the bunch creation process, when the laser pulse hits the photocathode. A precise control of the laser pulse would help to generate the desired electron bunch [2, 3], providing a valuable actuator towards the autonomous operation of accelerators [4]. Earlier approaches to laser pulse shaping often use fixed masks based on micro-lithographic techniques. Although they can achieve high fidelity pulse shaping, new masks need to be fabricated each time for different experiments [5]. In contrast, spatial light modulators (SLM) are programmable and allow flexible laser pulse shaping [6, 7]. An SLM is essentially a pixelated device with liquid-crystal (LC) filled cells. For a given voltage, the LC molecules in the SLM rotate and result in spatial modulation for phase, amplitude, or both. In this paper we focus on the phase-only case. One type of modern reflective SLM is based on the LCoS (liquid crystal on silicon) technique and can be simply used as a second monitor when connected to a computer. The SLM shapes the laser light according to a computer-generated hologram (CGH), which is often calculated with the Gerchberg–Saxton (GS) algorithm [8]. The wavefront of the light reflected from the SLM is shifted in phase according to the displayed hologram, and the modulated laser pulse shape can be reconstructed on the image plane.

The simplified layout of the FLUTE laser system is shown in Fig. 1. The uncompressed 800 nm Ti:Sa laser pulses are transported to the experimental hall over about 35 m. They are compressed for the third harmonic generation (THG) producing the 266 nm UV laser pulses required by the FLUTE photocathode and then stretched again by quartz rods. The beam is split directly before the cathode and one beam is guided to the virtual cathode as a diagnostic for the final laser pulse shape. Liquid crystals are susceptible to degradation with decreasing wavelengths towards the UV region. Thus, we placed an SLM in the 800 nm section before the THG, see Fig. 1. The simple Fourier transform-based GS algorithm is not sufficient to generate the proper CGH for laser manipulation, as it has no awareness of the nonlinear transformations after the SLM, including the THG and the pulse stretcher, which can distort the modulation. Recently, machine learning (ML) approaches have been introduced for CGH computations and achieved better image quality than traditional methods such as the GS algorithm [9–11]. Based on these promising results, we use a deep convolutional neural network (CNN) to learn the optical propagation between the SLM plane and the image plane as a first step. Such a CNN can be extended to the FLUTE laser setup as shown in Fig. 1 and use both, the laser and electron diagnostics as feedback. Combined with the GS algorithm, it can mitigate the non-linear distortions and improve the laser pulse shaping results.

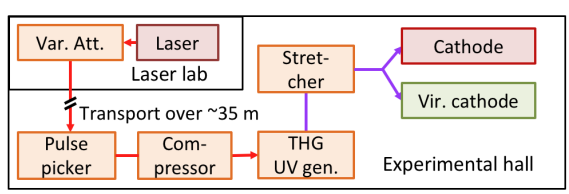

Figure 1: Simplified FLUTE laser layout [12].

In this paper, we present two test setups for the transverse and longitudinal laser pulse shape modulation with a commercially available phase-only SLM (model: Hamamatsu

* chenran.xu@kit.edu

ISBN: 978-3-95450-214-1 ISSN: 2673-5490 doi:10.18429/JACoW-IPAC2021-WEPAB289

LCoS-SLM X13138-02, wavelength: (800±50) nm, pixels: 1024 × 1272). Then, we experimentally demonstrate our CNN-GS method with the transverse test setup.

LASER MANIPULATION WITH SLM

Transverse Manipulation

The setup for transverse laser manipulation is shown in Fig. 2. The collimated 638 nm test laser first passes through a polarization filter, generating horizontally polarized light required by the SLM. Next, there is a telescope consisting of two lenses to expand the laser and fully utilize the SLM's active area. After reflection and modulation by the SLM, the laser is focused onto the screen and the image is captured by a camera (model: Basler ace, pixels: 2048 × 2448). A screen photo of a resulting transverse laser beam manipulation achieved with this setup is shown in Fig. 3. The zeroth order diffraction (ZOD) visible on the image is undiffracted light that does not interact with the CGH (specular reflection), resulting primarily from dead areas between pixels on the SLM surface or window reflections. The zeroth order should be less significant when working with the FLUTE driving laser, which is inside the working range of the SLMs, and can be further reduced or completely eliminated with various methods [13].

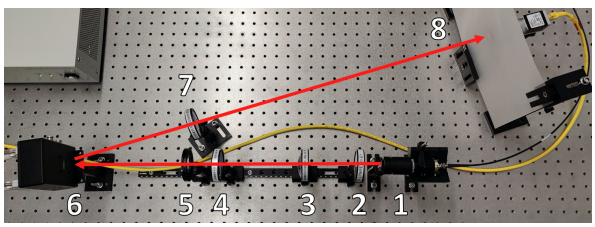

Figure 2: Test setup for transverse laser manipulation with a 638 nm laser (1). The red line depicts the laser path. (2) Horizontal polarization filter. (3, 4) $f = 150$ mm, $f = 100$ mm lens. (5) Iris. (6) SLM. (7) $f = 500$ mm lens. (8) Screen with the camera behind.

Figure 3: Photo of the transversely shaped laser on the screen of the test setup shown in Fig. 2. The zeroth order diffraction is visible in the center.

Longitudinal Manipulation

Conventional longitudinal modulation methods, for example using mechanical delay stages, allow only limited manipulation of fs-scale ultra-short laser pulses, often not sufficiently fast for intra-pulse modulation. A better and common method utilizes the chirp of a laser pulse, i.e. the correlation of time and wavelength. In this scheme, the chirped pulse is first dispersed spectrally, for example with a grating, then modulated in the spectral domain, and finally reassembled. Due to the wavelength-time correlation, a manipulation in the spectral domain does directly influence the time domain. Such a modulation can be achieved with a 4*f*-system, where the modulation mask, here the SLM, is located in the focal plane [6, 14, 15]. In our case, the laser pulse is linearly chirped with a spectral range of 750 nm to 850 nm. The setup is shown in Fig. 4. The laser pulse passes through a transmission optical grating with 600 lines/mm where it is split-up according to the wavelength and focused with a cylindrical lens $f = 250$ mm in the horizontal plane onto the SLM mask surface. The spectrogram on the SLM can now be modified in phase and is then reflected back passing through an identical cylindrical lens and an identical transmission grating, where the divergence of the wavelength spectrum is collimated.

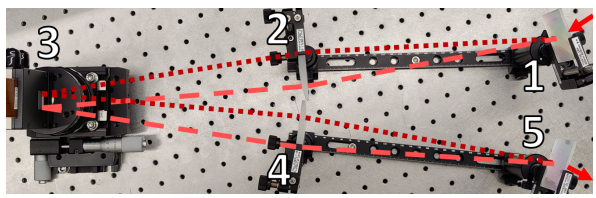

Figure 4: Photo of the longitudinal laser manipulation setup. The short dotted line represents 850 nm and the long dotted 750 nm wavelength. (1,5) Transmission optical grating 600 lines/mm. (2,4) $f = 250$ mm cylindrical lens. (3) SLM.

MACHINE LEARNING BASED CONTROL

To generate a laser pulse with an intensity pattern y_{target}, a CGH $\mathcal{G}(y_{\text{target}})$ is calculated using the GS algorithm and displayed on the SLM. The pulse, modulated by the SLM, further propagates through the optical path $\mathcal{P}$ to the image plane and is captured with an intensity pattern y. Thus, the forward mapping $\mathcal{F}$ of the intensity patterns can be written as a composite function of $\mathcal{G}$ and $\mathcal{P}$

$$y = \mathcal{F}(y_{\text{target}}) = \mathcal{P} \circ \mathcal{G}(y_{\text{target}}). \quad (1)$$

The unknown optical propagation $\mathcal{P}$ needs to be modeled, so that the y_{target} can be reproduced on the image plane. However, learning the inverse process $\mathcal{P}^{-1}$ directly is difficult, as it requires the network to learn the Fourier transform process. In the following we use an alternative route: train a CNN to learn the inverse process $\mathcal{F}^{-1}$ between the target image and the image plane.

Network Structure

We use a network structure inspired by the U-Net, which is originally used for image segmentation tasks [16]. As shown in Fig. 5, the input image is first sequentially downsampled to extract the features and then upsampled back to the original resolution for the predictions. C denotes the number of the convolution channels and N^2 is the pixel count. The downsampling layers and upsampling layers of the same depth are skip-connected to aid the training.

ISBN: 978-3-95450-214-1 ISSN: 2673-5490 doi:10.18429/JACoW-IPAC2021-WEPAB289

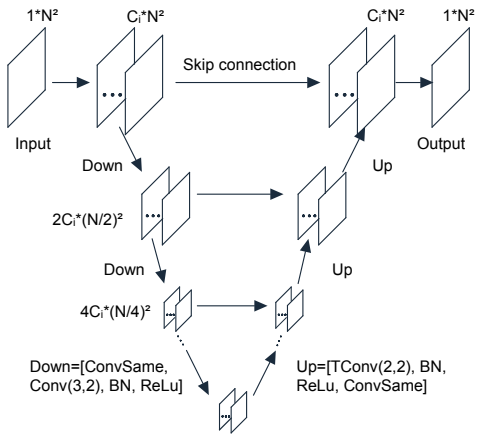

Figure 5: Structure of the CNN. The network consists of sequential downsampling and upsampling blocks, which are skip-connected. C: numbers of the convolution channels; N^2: resolution of the image; BN: Batch Normalization; ReLu: Rectified Linear Unit activation.

The definitions of the network layers and blocks are as follows: BN is a 2D batch normalization layer [17]; ReLu is the rectified linear unit activation function; $\mathrm{Conv}(K, S)$ is the 2D convolution layer with kernel size K and stride S; $\mathrm{TConv}(K, S)$ is the transposed 2D convolution layer. The ConvSame block consists of a Conv(3,1) and a BN layer, which changes the number of convolution channels and preserves the pixel count. It is used for processing the input image and predicting the output image. The "Down" block reduces the image resolution and increases the number of channels C, whereas the "Up" block does the opposite.

Training and Results

As a proof of principle experiment, we use the transverse setup described above and train the network on images with low pixel count $N^2 = 32^2$. The number of the initial channels is set to $C_i = 16$ and four downsampling layers are used, corresponding to 256 channels at the deepest layer. The training data is generated with images of handwritten digits from the MNIST database [18]. First, the original image with resolution of 28^2 is zero-padded to 32^2. Then a CGH is calculated by the GS algorithm and displayed on the SLM and the resulting laser image is captured. Lastly, the camera image is cropped to the region of interest and re-scaled to the same resolution as the target image $N^2 = 32^2$. The network is trained on 10,000 data pairs. We use Adam optimizer [19] with an initial learning rate 0.001, a mini-batch size of 32 and maximum 100 epochs. The loss function is defined as the mean squared error between the network-predicted image and target image. The trained CNN is used to produce three input laser patterns (a): a digit, a Gaussian beam and a flattop beam, as shown in Fig. 6. It is visible in (b) that the network could learn the physical distortions and attempts to suppress the zeroth order diffraction in the prediction. Compared to the simple GS method results (f), the

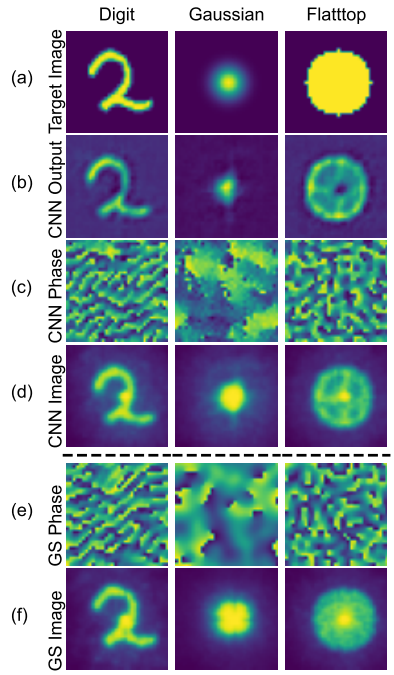

Figure 6: Experimental results of the laser shaping. (a) Target patterns/input of the CNN: digit (left), Gaussian (middle) and flattop (right). (b) Output patterns of the CNN. (c) Holograms corresponding to the CNN predictions and (d) the camera-captured patterns. (e) GS-only holograms and (f) the captured images.

shape results of the CNN-GS method (d) show somewhat suppressed ZOD. It is expected that the modulation quality can be further improved when using more pixels. The CNN can easily be extended by adding more layers and changing the number of convolution channels.

SUMMARY AND OUTLOOK

We achieved a proof-of-concept transverse laser shaping setup, which is ready to be implemented in the 800 nm driving laser of the FLUTE photoinjector. The CNN-based method is experimentally demonstrated on this setup. The setup for the longitudinal laser pulse manipulation is built in a test environment. After further evaluation, both the transverse and the longitudinal setup will be implemented in the photoinjector laser path before the THG and conversion to the UV range. The laser diagnostics such as the virtual cathode and electron diagnostics such as the YAG:Ce screen for the transverse beam shape will be used as feedback for a ML-based control system to shape the electron bunches to the needs of future experiments.

ACKNOWLEDGEMENTS

This work is funded by the Initiative and Networking Fund by the Helmholtz Association (Autonomous Accelerator, ZT-I-PF-5-6). C. Xu acknowledges the support by the DFG-funded Doctoral School "Karlsruhe School of Elementary and Astroparticle Physics: Science and Technolog".

ISBN: 978-3-95450-214-1 ISSN: 2673-5490 doi:10.18429/JACoW-IPAC2021-WEPAB289

REFERENCES

[1] M. J. Nasse *et al.*, "FLUTE: A versatile linac-based THz source", *Rev. Sci. Instrum.*, vol. 84, no. 2, p. 022 705, 2013. doi:10.1063/1.4790431

[2] F. Zhou, A. Brachmann, P. Emma, S. Gilevich, and Z. Huang, "Impact of the spatial laser distribution on photocathode gun operation", *Phys. Rev. ST Accel. Beams*, vol. 15, p. 090 701, Sep. 2012. doi:10.1103/PhysRevSTAB.15.090701

[3] J. Maxson, H. Lee, A. C. Bartnik, J. Kiefer, and I. Bazarov, "Adaptive electron beam shaping using a photoemission gun and spatial light modulator", *Phys. Rev. ST Accel. Beams*, vol. 18, p. 023 401, Feb. 2015. doi:10.1103/PhysRevSTAB.18.023401

[4] A. Eichler *et al.*, "First Steps Toward an Autonomous Accelerator, a Common Project Between DESY and KIT", presented at the 12th Int. Particle Accelerator Conf. (IPAC'21), Campinas, Brazil, May 2021, paper TUPAB298, this conference.

[5] A. M. Weiner, J. P. Heritage, and E. M. Kirschner, "High-resolution femtosecond pulse shaping", *J. Opt. Soc. Am. B*, vol. 5, no. 8, pp. 1563–1572, Aug. 1988. doi:10.1364/JOSAB.5.001563

[6] A. M. Weiner, "Femtosecond pulse shaping using spatial light modulators", *Rev. Sci. Instrum.*, vol. 71, no. 5, pp. 1929–1960, May 2000. doi:10.1063/1.1150614

[7] C. Rosales-Guzmán and A. Forbes, *How to Shape Light with Spatial Light Modulators*. Bellingham, Washington, USA: SPIE PRESS, 2017.

[8] R. W. Gerchberg and W. O. Saxton, "A practical algorithm for the determination of phase from image and diffraction plane pictures", *Optik*, vol. 35, pp. 237–246, 1972.

[9] A. Sinha, J. Lee, S. Li, and G. Barbastathis, "Lensless computational imaging through deep learning", *Optica*, vol. 4, no. 9, pp. 1117–1125, Sep. 2017. doi:10.1364/OPTICA.4.001117

[10] R. Horisaki, R. Takagi, and J. Tanida, "Deep-learning-generated holography", *Appl. Opt.*, vol. 57, no. 14, p. 3859, 2018. doi:10.1364/ao.57.003859

[11] Y. Peng, S. Choi, N. Padmanaban, J. Kim, and G. Wetzstein, "Neural holography", in *Proc. ACM SIGGRA'20 Emerging Technologies*, Virtual Event, USA, Aug. 2020, pp. 1–2. doi:10.1145/3388534.3407295

[12] A. Malygin *et al.*, "Commissioning status of FLUTE", in *Proc. 9th Int. Particle Accelerator Conf. (IPAC'18)*, Vancouver, Canada, Apr.-May, 2018, pp. 4229–4231. doi:10.18429/JACoW-IPAC2018-THPMF068

[13] J. Liang, S.-Y. Wu, F. K. Fatemi, and M. F. Becker, "Suppression of the zero-order diffracted beam from a pixelated spatial light modulator by phase compression", *Appl. Opt.*, vol. 51, no. 16, pp. 3294–3304, Jun. 2012. doi:10.1364/AO.51.003294

[14] S. Y. Mironov *et al.*, "Shaping of cylindrical and 3d ellipsoidal beams for electron photoinjector laser drivers", *Appl. Opt.*, vol. 55, no. 7, pp. 1630–1635, Mar. 2016. doi:10.1364/AO.55.001630

[15] J. W. Goodman, *Introduction to Fourier optics*, 3rd ed. Englewood, CO, USA: Roberts & Co., 2005.

[16] O. Ronneberger, P. Fischer, and T. Brox, "U-net: Convolutional networks for biomedical image segmentation", 2015. arXiv: 1505.04597

[17] S. Ioffe and C. Szegedy, "Batch normalization: Accelerating deep network training by reducing internal covariate shift", in *Proc. 32nd International Conference on Machine Learning - Volume 37*, Lille, France, Jul. 2015, pp. 448–456.

[18] MNIST handwritten digit database, http://yann.lecun.com/exdb/mnist/.

[19] D. P. Kingma and J. Ba, "Adam: A method for stochastic optimization", 2015. arXiv: 1412.6980